IIETA International Information and Engineering Technology Association
Advancing the World of Information and Engineering

Mathematical Modelling of Engineering Problems
Vol. 12, No. 11, November, 2025, pp. 3963-3970
Journal homepage: http://iieta.org/journals/mmep

Ka4-55 Series Based Toroidal Propeller Design

Achmad Baidowi[1*], Riyan Bagus Prihandanu[1,2], Fadil Hafuza[1]

[1] Marine Engineering Department, Faculty of Marine Technology, Sepuluh Nopember Institut of Technology, Surabaya 60111, Indonesia
[2] Department of Marine Engineering, Shipbuilding Institute of Polytechnic Surabaya, Surabaya 60111, Indonesia

Corresponding Author Email: achmad.baidowi@its.ac.id

Copyright: ©2025 The authors. This article is published by IIETA and is licensed under the CC BY 4.0 license (http://creativecommons.org/licenses/by/4.0/).

https://doi.org/10.18280/mmep.121122

Received: 7 July 2025
Revised: 28 October 2025
Accepted: 12 November 2025
Available online: 30 November 2025

Keywords:
advance coefficient, CFD, Ka4-55, performance, toroidal propeller

ABSTRACT

Toroidal marine propellers have become a phenomenon in the propeller design world, as their design can enhance propeller performance exceeding conventional designs. Toroidal propeller blades typically feature a small Ae/A0 ratio and, relatively constant chord. One of Kaplan's propeller series, Ka4-55, has the required features and provides comprehensive open water test data. This study investigates the possibility of Ka4-55 being used as the base of a toroidal propeller and evaluates the performance using the CFD method. To conduct a more detailed analysis of which part contributes significantly to the performance, the blade area is divided into three sections: S1, close to the root area; S2, in the middle; and tip. The analysis indicates that toroidal propellers based on Ka4-55 provide high thrust for low to medium advance coefficient (J) and higher efficiency for higher advance coefficient (J) with a range of J > 0.8.

1. INTRODUCTION

Since the introduction of the toroidal propeller [1], there are numerous research and design proposals have been proposed for the development of the toroidal propeller. Sharrow has patented a design in the US Patent Office for its toroidal design called Duo-Prop Propeller [2], and the Massachusetts Institute of Technology (MIT) also developed a different model of toroidal propeller, while Li et al. [3] have developed the mathematical model of the toroidal propeller. This study introduces a new configuration referred to as the Toroidal propeller, developed by combining two coaxial blade systems connected at the tip to form a continuous looped geometry. This configuration is inspired by toroidal flow concepts but is structurally and functionally distinct, with a focus on improving thrust performance through tip integration. This closed-loop blade shape is designed to reduce tip vortices and improve flow uniformity behind the propeller. This unique configuration presents a potential breakthrough in propeller design, especially for applications requiring high maneuverability, lower noise levels [1, 4], and enhanced fuel efficiency.

Attar et al. [5] explain that the toroidal bionic propeller has low noise levels, high efficiency at low speeds, and reduced turbulence and tip vortices. A specific pitch will enhance efficiency, while the number of blades affects thrust, although its impact on efficiency is not significant [6, 7]. The toroidal propeller generates higher torque and lower noise, while the Wageningen B-Series propeller excels in thrust performance [8]. The closed-loop propeller has an efficiency improvement of 0.27–12.31% compared to conventional propellers [9, 10].

By integrating a dual coaxial blade system, further research can be conducted using specific series propellers. Modifications to the previous Kaplan propeller have been made. The angle of attack influences pressure distribution, and the number of blades tends to result in lower efficiency [6]. In studies, the variation in the angle of attack will be maximized at specific variations of the number of blades and diameter [8].

In this research, the Toroidal design was developed based on the Kaplan Ka4-55 series. The Ka4-55 was chosen for three main reasons: first, it features a four-blade configuration with the smallest Ae/Ao ratio among the Kaplan series [11]; second, the propeller's outline shape exhibits a relatively constant chord distribution across all r/R values, making it suitable for the closed-loop geometry envisioned in the Toroidal design; and third—and most importantly—it comes with comprehensive open-water test data from MARIN's ducted propeller program. To isolate true open-water behavior, all nozzle effects were removed, and the resulting thrust, torque, and efficiency data served as the benchmark for evaluating the toroidal configuration.

This study focuses on analyzing the performance of the toroidal propeller with P/D = 1.25, which was designed based on Ka4-55, compared to the original unducted Kaplan Ka4-55, using open water performance metrics—thrust coefficient (KT), torque coefficient (KQ), and open water efficiency—as the basis for evaluation. The goal is to understand whether the Ka4-55-based toroidal propeller is able to improve hydrodynamic performance while maintaining the original propeller Kaplan design.

2. METHODOLOGY

2.1 Propeller geometry and design parameters

A toroidal propeller consists of a front and a rear blade set, both derived from the Kaplan Ka4-55 series profile. The front and rear blades are designed with an Expanded Area Ratio (EAR) of 0.55. Both blades have identical chord lengths of 62.2 mm, and this blade is connected at its tips through a parabolic rake geometry, forming a continuous closed-loop shape [12]. The rear blade is rotated by a 15° generator line angle relative to the front blade to improve alignment with the flow path and simplify the tip integration.

The skew distribution applied to the front blade follows the pattern used in the B-Series propellers, with a total skew angle of 20.44°. The rake is applied parabolically, with a maximum rake angle of 30°, providing a smooth axial displacement between the front and rear blades. The detailed drawings of the front and rear blades are presented in Figures 1 and 2, respectively. A three-dimensional view of the blades before connection is shown in Figure 3, while the complete toroidal configuration is illustrated in Figure 4. These geometric adjustments support the structural connection at the blade tips and assist in shaping the propeller into an integrated, looped configuration.

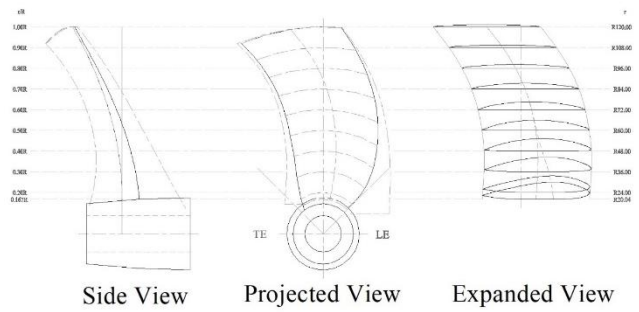

Figure 1. Front side toroidal propeller design

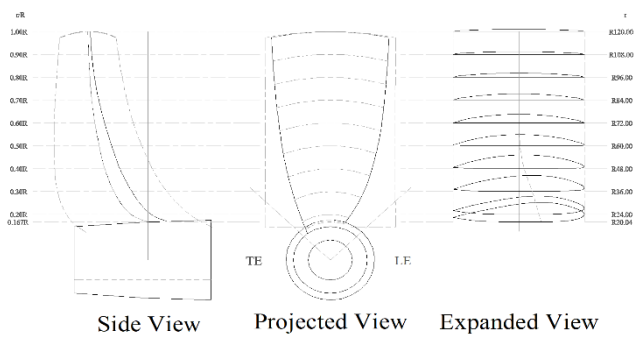

Figure 2. Back side toroidal propeller design

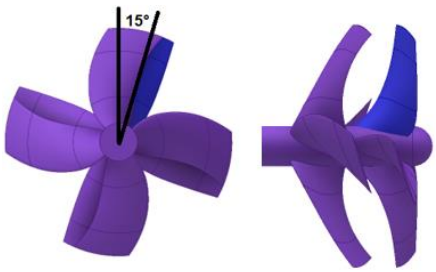

Figure 3. Front and back toroidal propeller design

Figure 4. 3D model of toroidal design

Figure 5. Toroidal foil profile at 0.2 R

Figure 6. Toroidal foil profile at 0.4 R

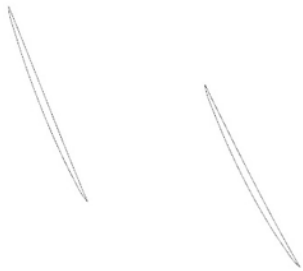

Figure 7. Toroidal foil profile at 0.8 R

The tips of the blades are truncated at r/R = 0.8, enabling a smooth structural connection between front and rear blade tips. This configuration forms the defining feature of the toroidal design: a seamlessly joined blade loop intended to reduce tip vortex and enhance propeller efficiency. The pitch ratio (P/D) of the front blade is fixed at 1.0, while the rear blade uses a P/D ratio Of 1.25. The pitch distribution is kept identical to that of the original Kaplan series.

The left side of Figures 5-7 corresponds to the upstream (inflow) region, while the right side represents the downstream (outflow) region. The geometry resulting from the intersection of the front and rear propeller foils in the toroidal configuration exhibits a distinct arrangement, as illustrated in Figures 5-7. In this design, the rear propeller blades are not positioned in line with the front propeller blades. Consequently, the downstream flow generated by the front propeller is not directly utilized by the rear propeller in a conventional tandem manner. Additionally, the spacing between the foils increases progressively toward the upper region of the blade. This configuration is intentionally applied to create a smoother connection between the blade tips, ensuring a continuous and seamless transition for the toroidal propeller shape. This gradual variation in spacing is aimed at minimizing flow separation and optimizing the overall hydrodynamic performance of the toroidal propeller system.

2.2 CFD setup

In modeling turbulent fluid flow around a propeller, the Reynolds-Averaged Navier–Stokes (RANS) equations are commonly employed to capture the variations in flow velocity, pressure, and vorticity [13, 14]. These equations, derived from the Navier–Stokes formulation, consider the advection and diffusion mechanisms that significantly influence the temporal change of velocity distribution around the propeller.

$$\frac{\partial u_i}{\partial x_i} = 0 \tag{1}$$

$$\frac{\partial u_i}{\partial t} + \frac{\partial u_i u_j}{\partial x_i} = -\frac{1}{\rho}\frac{\partial P}{\partial x_i} + \frac{\partial}{\partial x_j}\left(\frac{\mu \partial u_i}{\partial x_j}\right) + \frac{\partial}{\partial x_i}\left(\mu \frac{\partial u_i}{\partial x_j}\right) - \frac{\partial}{\partial x_j}\left(-\rho \overline{u_i' u_j'}\right) \tag{2}$$

Advection accounts for the movement of fluid itself, while diffusion represents the effects of fluid viscosity. As noted in the formulation:

$$\frac{\partial}{\partial x_j}\left(\mu \frac{\partial u_i}{\partial x_j}\right) + \frac{\partial}{\partial x_k}\left(\mu \frac{\partial u_i}{\partial x_k}\right) \tag{3}$$

These terms describe how changes in momentum and velocity gradients occur due to internal fluid stresses. Additionally, the pressure gradient term, $-\frac{\partial p}{\partial x_j}$ plays a critical role in driving the flow dynamics.

The k-omega turbulence model is a widely used RANS-based approach that solves two additional transport equations for turbulent kinetic energy (k) and specific dissipation rate (ω), representing turbulence energy and its dissipation. The dissipation rate is defined as $\varepsilon = \beta \cdot k\omega$, with $\beta = 0.09$. Variants such as the standard, BSL, and SST k-omega models offer improved performance for specific flow conditions [15].

$$\epsilon = C_\mu k\omega \tag{4}$$

Transport equation for turbulent kinetic energy (k) is given as follows:

$$\frac{\partial(\rho\epsilon)}{\partial t} + \frac{\partial(\rho U_i \epsilon)}{\partial x_i} = \frac{\partial}{\partial x_j}\left[\left(\mu + \frac{\mu_t}{\sigma_\epsilon}\right)\frac{\partial \epsilon}{\partial x_j}\right] + \frac{\gamma}{\nu_t} P_k - \beta\rho\omega^2 + \frac{2\rho\sigma_\omega^2}{\omega}\Delta k : \Delta\omega \tag{5}$$

where,

$$\Delta k : \Delta\omega = \frac{\partial k}{\partial x_j}\frac{\partial \omega}{\partial x_j} \tag{6}$$

The term,

$$\frac{2\rho\sigma_\omega^2}{\omega}\Delta k : \Delta\omega \tag{7}$$

The hydrodynamic performance of the toroidal propeller was analyzed using CFD simulations under steady-state conditions. The flow was assumed to be incompressible, and the governing equations used were the RANS equations. Turbulence effects were modeled using a two-equation model capable of handling adverse pressure gradients and flow separation, which are critical phenomena around marine propellers [16-19].

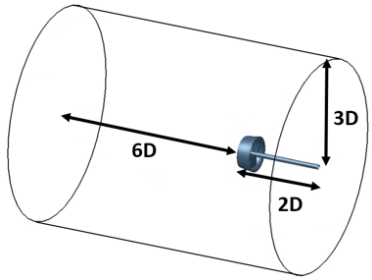

Figure 8. Domain size

The computational domain was created in accordance with the guidelines provided by the International Towing Tank Conference (ITTC) for open water propeller simulations. The upstream distance from the propeller to the inlet boundary was set to at least 2D, the downstream outlet extended to 6D, where D is the propeller diameter. The radial boundary distance from the axis of rotation to the domain wall was set to 3D, ensuring minimal blockage and reflecting realistic open water conditions (Figure 8) [20].

An unstructured mesh was generated with local refinement around the propeller blades and wake region. Mesh independence studies were conducted to verify that further mesh refinement did not significantly influence the simulation results. Boundary conditions included a uniform inflow velocity, a fixed rotational speed for the propeller, and a static pressure outlet to emulate an open water environment.

To ensure the reliability of the numerical method, simulation results for the benchmark Kaplan Ka4-55 propeller were compared against available open water test data. The comparison focused on KT, KQ, and open water efficiency. The CFD predictions showed acceptable accuracy, with deviations under 5% for KT and 10% for KQ [13, 20], which are consistent with ITTC-recommended tolerances for numerical validation in open water propeller analysis.

2.3 Propeller geometry and design parameters

The characteristics of ship propellers can be expressed in non-dimensional form using the advance coefficient (J), thrust coefficient (K_T), torque coefficient (K_Q), and efficiency (η) [21, 22]. These three coefficients are used to construct performance curves that illustrate how the propeller operates under various ship operating conditions. Variations in the K_T and K_Q curves with respect to changes in the advance ratio provide insights into the propeller's performance in relation to ship speed and propeller rotation. Each type of propeller has its own unique performance curve characteristics; therefore, the study of propeller characteristics cannot be generalized to all shapes or types of propellers [23].

$$J = \frac{V_a}{nD} \tag{8}$$

$$K_T = \frac{T}{\rho n^2 D^4} \tag{9}$$

$$K_Q = \frac{Q}{\rho n^2 D^5} \tag{10}$$

$$\eta = \frac{JK_T}{2\pi K_Q} \quad (11)$$

In this context, T is thrust (N), Q is torque (Nm), ρ is water density (kg/m³), n is rotational speed (rad/s), and D is propeller diameter (m).

3. RESULTS

3.1 Validation with experimental data

To validate the CFD methodology, simulations are first performed on the Kaplan Ka4-55 propeller with a nozzle, replicating the conditions of available experimental data. The CFD results for KT, KQ, and open water efficiency are compared against the experimental measurements. Table 1 shows good agreement with an error of less than 10% [20], with discrepancies within acceptable limits, thereby confirming the accuracy of the CFD setup for predicting propeller performance.

Table 1. Performance difference with experiment data

J	KT Difference	10KQ Difference	Eff. Difference
0.3	1.52%	8.89%	2.83%
0.4	1.44%	9.27%	3.61%
0.5	-2.72%	3.28%	3.24%
0.6	-3.98%	5.73%	5.27%

3.2 Unducted propeller performance

To establish a baseline for evaluating the performance of modified propeller designs, a simulation was conducted on the Kaplan Ka4-55 propeller without its nozzle. Removing the nozzle allows the analysis to focus solely on the propeller's inherent hydrodynamic characteristics, without any external enhancement from ducting effects. The results of this simulation, as presented in Figure 9, show that the unducted Ka4-55 propeller achieves a higher maximum efficiency under open water conditions compared to its ducted version. However, at lower advance coefficient values, the ducted configuration demonstrates superior efficiency. This is because the nozzle plays a significant role in accelerating the incoming flow when the ship is operating at low speeds, thereby increasing the generated thrust.

Since the unducted Ka4-55 provides higher performance during high advance coefficients where the toroidal propeller is expected to operate, the unducted Ka4-55 was selected as the base model for further modifications. Following this, the unducted Ka4-55 propeller was compared with the redesigned front and rear blades intended for the toroidal propeller configuration. This comparison aimed to assess the effects of specific geometric modifications, such as adjustments in chord length, rake angle, and skew distribution, on the overall propeller performance. The simulation results, shown in Tables 2-4, show a modest increase in efficiency, ranging from 0.3% to 1%, in the modified blade designs. However, individual modifications to skew, rake, and chord alone did not produce significant improvements in open water efficiency. When focusing on thrust and torque, the original unducted Ka4-55 propeller consistently delivered the highest KT and KQ values, with differences ranging from 1–8% for KT and 1–9% for KQ compared to the modified designs.

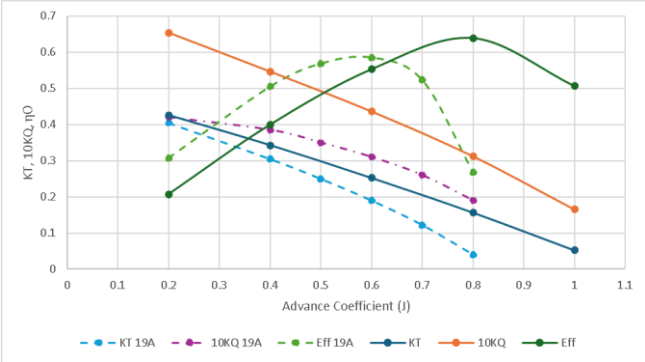

Figure 9. Comparison of Ka4-55 using the nozzle and without the nozzle

Table 2. Simulation results Ka4-55

J	KT	KQ	10KQ	Eff
0.2	0.425601	0.065355	0.65355	20.7%
0.4	0.342903	0.054631	0.546306	40.0%
0.6	0.252416	0.043611	0.436114	55.3%
0.8	0.156766	0.031239	0.312388	63.9%
1	0.052704	0.016565	0.165646	50.7%

Table 3. Simulation results of the front propeller

J	KT	KQ	10KQ	Eff
0.2	0.392189	0.059361	0.593605	21.0%
0.4	0.320782	0.05058	0.505803	40.4%
0.6	0.239525	0.041032	0.410324	55.8%
0.8	0.151092	0.029988	0.299881	64.2%
1	0.051184	0.01597	0.159703	51.0%

Table 4. Simulation results of the back propeller

J	KT	KQ	10KQ	Eff
0.2	0.406832	0.061362	0.613621	21.1%
0.4	0.331507	0.051965	0.51965	40.6%
0.6	0.247177	0.042128	0.421276	56.1%
0.8	0.155994	0.030611	0.306114	64.9%
1	0.053166	0.016391	0.16391	51.7%

3.3 Toroidal propeller design based on Ka4-55

The propeller blade tips were trimmed at a radial position of r/R = 0.8 to enable a structural connection with the tips of the adjacent blades, forming a continuous closed-loop geometry as illustrated in Figure 4. Based on the simulation results, the original Ka4-55 propeller consistently achieved higher overall open-water efficiency compared to the integrated configuration, in which the pitch of the rear blade was modified. However, the toroidal propeller demonstrated noticeably higher thrust and torque coefficients across most advanced coefficient values, indicating increased load generation because of the integrated blade arrangement.

These findings indicate that combining two blades into a single propeller does not simply double its performance. Instead, the structural connection at the blade tip introduces significant geometric changes that affect the flow and force distribution. It is well known that the blade tip region contributes the most to thrust generation, despite typically exhibiting the lowest efficiency. This is further confirmed by the segmental analysis presented in Table 5 and the segment layout shown in Figure 10. The root region of the blade was found to contribute minimally to thrust, serving primarily as a

structural role for mechanical support.

Therefore, any modifications applied to the tip—especially in configurations such as the toroidal propeller—must be carefully evaluated, as they have a direct influence on the resulting thrust and torque characteristics of the propeller system.

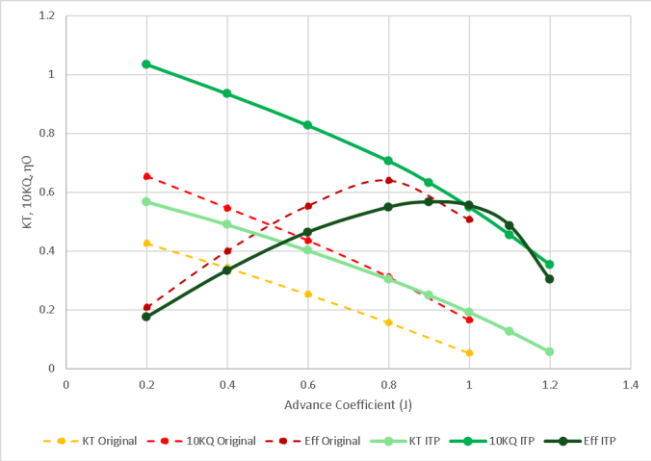

Figure 10. Comparison performance original and toroidal diagrams

The results of the comparison of open water performance between the Ka4-55 propeller and the toroidal showed a contrasting performance pattern at low to medium advance coefficient values (J = 0.2–0.6). At J = 0.2, toroidal yields a thrust coefficient (KT) of 0.567992, which is higher than Ka4-55 at 0.425601. However, the torque coefficient (10KQ) of toroidal reaches 1.034857, which is much higher than Ka4-55's of 0.65355. This affects the efficiency of the toroidal propeller, which is actually lower (17.5%) than the Ka4-55 (20.7%), even though the thrust value is larger. This phenomenon also occurs at J = 0.4 and J = 0.6, where even though toroidal has a superior KT. A very high increase in torque will decrease efficiency significantly.

The pattern began to change at J = 0.8 and J = 0.9, where the toroidal efficiency began to overtake Ka4-55, 54.9% vs. 63.9% at J = 0.8, and 56.7% vs. 50.7% at J = 0.9, respectively. This trend shows that toroidal tends to be more optimal at the high advance coefficient, where the torque load can be more balanced with the thrust generated. The initial hypothesis states that the looped-tip geometry on toroidal significantly increases thrust at low J but causes torque overloading due to complex flow interactions between the front and rear blades. At high J, the effect of the flow interaction becomes more stable, so that the propeller provides higher efficiency. These conditions require more comprehensive analysis through pressure distribution and wake visualization to confirm the effect of looped-tip and tandem configurations on load distribution patterns along the J range [22, 24, 25].

4. DISCUSSION

4.1 Segmented blade analysis

Based on the results, the toroidal simulation provides efficiency but has a wider range of advanced coefficients. However, the main problem is that the torque required by the propeller reaches almost 2 times greater than the torque of the Ka4-55 propeller. This makes the overall toroidal have no advantages. Therefore, further analysis is needed regarding the cause of this propeller becoming more labor-intensive than its original form.

The performance of the Ka4-55 propeller is getting worse than that of the Ka4-55, so the propeller is made into several segments as shown in Figure 11. From this segment, it is known that the root part of the propeller does not have a significant impact on the thrust of the propeller. So that this part functions more as a propeller blade amplifier. When the tip section is modified in such a way, the potential thrust and torque values will also change.

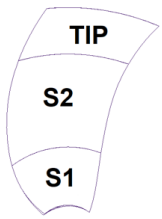

Figure 11. Propeller segmentation

Table 5. KT propeller simulation results (1 blade)

J	S1 Area			S2 Area			Tip Area	
	Ka4-55	Toroidal Prop		Ka4-55	Toroidal Prop		Ka4-55	Toroidal Prop
		Front	Rear		Front	Rear		
0.2	0.0071	0.0074	-0.0026	0.0502	0.0434	0.0269	0.0515	0.0684
0.4	0.0065	0.0065	-0.0014	0.0438	0.0364	0.0269	0.0372	0.0557
0.6	0.0052	0.0051	-0.0003	0.0343	0.0280	0.0259	0.0246	0.0429
0.8	0.0033	0.0031	0.0007	0.0225	0.0175	0.0250	0.0137	0.0304
1	0.0007	0.0003	0.0018	0.0084	0.0041	0.0240	0.0040	0.0180

Table 6. 10KQ propeller simulation results (1 blade)

J	S1 Area			S2 Area			Tip Area	
	Ka4-55	Toroidal Prop		Ka4-55	Toroidal Prop		Ka4-55	Toroidal Prop
		Front	Rear		Front	Rear		
0.2	0.00973	0.00991	-0.00252	0.07120	0.06212	0.05843	0.08244	0.13002
0.4	0.00949	0.00959	-0.00021	0.06551	0.05598	0.05796	0.06155	0.11050
0.6	0.00849	0.00845	0.00181	0.05607	0.04790	0.05649	0.04449	0.09219
0.8	0.00640	0.00620	0.00380	0.04228	0.03535	0.05572	0.02938	0.07549
1	0.00299	0.00251	0.00582	0.02335	0.01727	0.05480	0.01507	0.05707

Table 7. Propeller efficiency (1 blade)

J	S1 Area			S2 Area			Tip Area	
	Ka4-55	Toroidal Prop		Ka4-55	Toroidal Prop		Ka4-55	Toroidal Prop
		Front	Rear		Front	Rear		
0.2	0.00973	0.00991	-0.00252	0.07120	0.06212	0.05843	0.08244	0.13002
0.4	0.00949	0.00959	-0.00021	0.06551	0.05598	0.05796	0.06155	0.11050
0.6	0.00849	0.00845	0.00181	0.05607	0.04790	0.05649	0.04449	0.09219
0.8	0.00640	0.00620	0.00380	0.04228	0.03535	0.05572	0.02938	0.07549
1	0.00299	0.00251	0.00582	0.02335	0.01727	0.05480	0.01507	0.05707

The results in Tables 5-7 of the open water simulation showed an interesting performance pattern while leaving anomalies, especially in the rear toroidal blade in low advance coefficient conditions (J = 0.2 and 0.4). Under these conditions, the rear blade toroidal produces a negative thrust coefficient (KT) value of up to -0.0026, indicating an obstacle force compared to thrust. This statement is supported by the pressure distribution shown in Figure 12, where the back propeller exhibits negative values and significantly lower pressure compared to the front propeller. This phenomenon is amplified by the torque coefficient (10KQ) of the rear blade, which is close to zero or even negative, which generally occurs due to unstable flow or local stalls in certain areas of the blade. This situation is inversely proportional to the tip blade of toroidal, which shows a significant increase in performance compared to the conventional propeller Ka4-55, both in terms of KT, 10KQ, and efficiency in the entire J range, especially at the high advance coefficient.

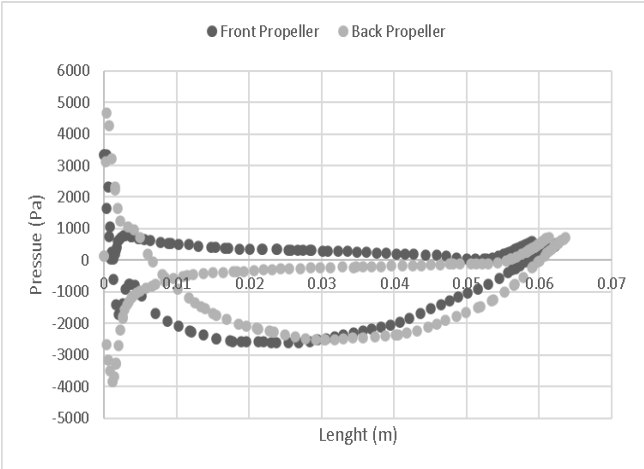

Figure 12. Pressure distribution of 0.375 r/R

The condition of the rear blade that experienced negative performance at low J is suspected to be caused by a suboptimal flow interaction between the front and rear blade, so that the rear blade receives the remaining flow (wake) with too high an angle of attack. The initial hypothesis states that the equal pitch distribution between the front and rear blades and the P/D = 1.25 configuration may cause the rear blade to overload in low J conditions. Therefore, further evaluation of pressure distribution, wake flow patterns, and possible pitch or angle of attack adjustments on the rear blade is needed to optimize performance at low advance coefficients without sacrificing efficiency advantages at high J.

4.2 Flow visualization and interpretation

From the visualization image of the X-axis relative flow velocity, the difference in speed distribution between the conventional Ka4-55 propeller and the toroidal propeller in both radial positions can be seen. At the position r/R = 0.75, as shown by Figures 13 and 14, the difference becomes more pronounced. The Ka4-55 propeller still shows a sharp, symmetrical wake tip around the blade tip. In contrast, in toroidal, two wake streams converge in the blade tip area due to the integration between the blades, with a larger wake area and a low-speed flow (blue-green color) spreading more backwards. This can indicate a more intense wake interaction and a potential vortex tip reduction due to the splicing of the blade tip.

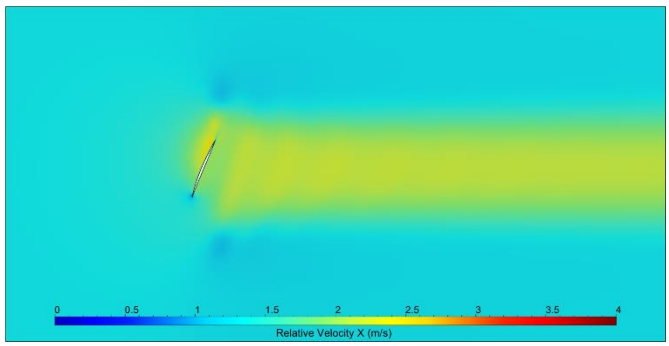

Figure 13. Ka4-55 0.75 r/R

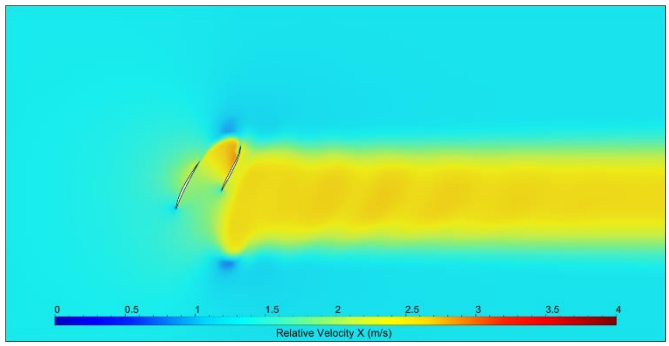

Figure 14. Toroidal propeller 0.75 r/R

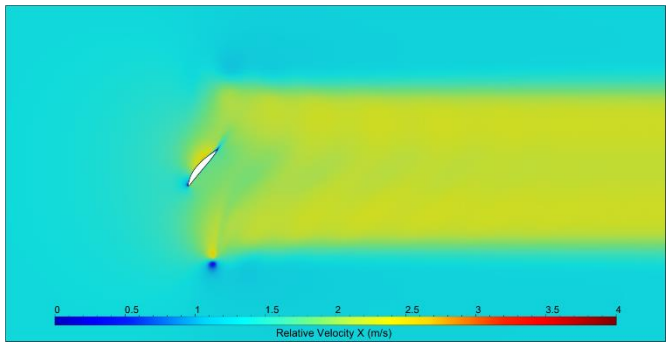

Figure 15. Ka4-55 0.375 r/R

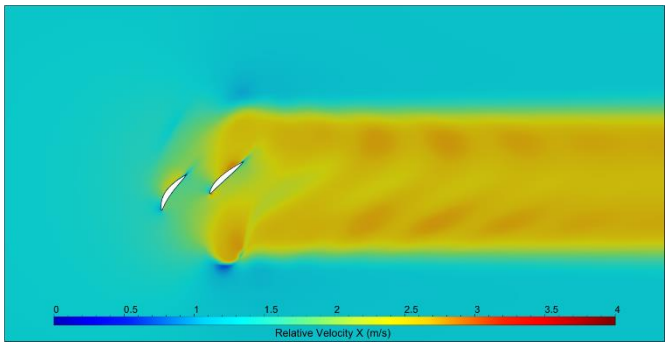

Figure 16. Toroidal propeller 0.375 r/R

At the r/R = 0.375 position, the flow around the Ka4-55 propeller shows a relatively uniform velocity distribution around the blades as described in Figures 15 and 16, with the wake area behind the propeller being concentrated. Meanwhile, in toroidal, there are two separate wake distributions due to the presence of integrated front and rear blades, where the wake or turbulence from the front blades slightly interacts with the rear-blade, resulting in a wider and more complex distribution of speed.

5. CONCLUSION

The study found that the toroidal propeller produces higher thrust and torque coefficients than the original unducted Ka4-55 propeller, particularly at low to medium advance coefficients. However, this comes with a significant increase in torque demand, which reduces overall efficiency at low J values. Efficiency improvements for the toroidal propeller only become noticeable at higher advance coefficients ($J \geq 0.8$), where wake flow interactions become more stable, and the propeller operates more effectively.

Section analysis confirmed that the blade tip remains the largest contributor to thrust generation, while the rear blade of the toroidal propeller exhibited negative thrust and low torque performance at low advance coefficients due to suboptimal flow interactions and excessive angle of attack. Flow visualizations further supported these findings, showing wider wake areas and better potential for tip vortex reduction in the toroidal configuration.

In conclusion, while the toroidal propeller shows potential benefits in thrust generation and wake control, especially at high advance coefficients, it requires further optimization of pitch, angle of attack, and rear blade load distribution to address its efficiency limitations at lower speeds.

ACKNOWLEDGMENT

The authors would like to thank Marine Manufacturing and Design (MMD) Laboratory of Marine Engineering, Sepuluh Nopemebr Institut of Technology for the Software License.

REFERENCES

[1] Xu, P., Guo, Y., Ye, L., Song, K. (2024). Hydrodynamic performance of toroidal propeller based on detached eddy simulation method. Journal of Marine Science and Engineering, 12(12): 2132. https://doi.org/10.3390/jmse12122132

[2] Sharrow, G.C. (2022). Duo-Propellers and Single Publication Classification Propellers. US Patent Application. https://patentimages.storage.googleapis.com/e9/62/7a/035c1a72bdaf11/US20220340247A1.pdf.

[3] Li, Y.Y., Wang, C., Sun, C., Guo, C.Y. (2024). Mathematical expression method for geometric shape of toroidal propeller. Chinese Journal of Ship Research, 19(3): 224-233. https://doi.org/10.19693/j.issn.1673-3185.03419

[4] Diatmaja, H., Prabowo, A.R., Adiputra, R., Muhayat, N., Baek, S.J., Huda, N., Tuswan, T., Zubaydi, A., Nubli, H. (2023). Comparative evaluation of design variations in prototype fast boats: A hydrodynamic characteristic-based approach. Mathematical Modelling of Engineering Problems, 10(5): 1487-1507. https://doi.org/10.18280/mmep.100501

[5] Attar, A.R., Mane Deshmukh, S.B., Shinde, A. (2025). Advancements in marine propulsion: Design, development, and testing of a bionic-toroidal propeller. https://imare.in/wp-content/uploads/2025/02/30-Advancements-in-Marine-Propulsion-Design-Development-and-Testing-of-a-Bionic-Toroidal-Propeller_Ajaj-Attar.pdf.

[6] Sinaga, N., Dhande, D.Y., Yunianto, B. (2022). A numerical investigation of the effect of blade number on the performance of an INSEAN E779A marine propeller in a cavitating flow using computational fluid dynamics. Ocean Engineering, 261: 112063. https://doi.org/10.1016/j.oceaneng.2022.112063

[7] Bouregba, F., Belkadi, M., Aounallah, M., Adjlout, L. (2019). Effect of the blade number on the marine propeller performance. EPJ Web of Conferences, 213: 02007. https://doi.org/10.1051/epjconf/201921302007

[8] Putraa, B.A., Rayhan, F.A., Sugeri, M. (2026). Comparative analysis of conventional and toroidal propeller through CFD methods. CFD Letters, 18(2): 137-160. https://doi.org/10.37934/cfdl.18.2.137160

[9] Alm, A., Garrison, W.P., Gomes, V.R., Harris, C.H., Shrauger, G.T., Whitacre, C., Matsson, J.E. (2024). A study of the efficiency of toroidal propeller designs. In 2024 ASEE Annual Conference & Exposition, Portland, Oregon. https://doi.org/10.18260/1-2--46494

[10] Hassan, H.M., Elsakka, M.M., Moustafa, M.M. (2024). On the comparative hydrodynamic analysis of conventional and innovative closed-loop marine propellers [Preprint]. Research Square. https://doi.org/10.21203/rs.3.rs-4814004/v1

[11] Liu, B., Vanierschot, M. (2021). Numerical study of the hydrodynamic characteristics comparison between a ducted propeller and a rim-driven thruster. Applied Sciences, 11(11): 4919. https://doi.org/10.3390/app11114919

[12] Ciftci, O., Cadirci, S. (2024). Multi-objective optimization for performance enhancement of a toroidal propeller using CFD and FSI. In ASME 2024 International Mechanical Engineering Congress and Exposition, IMECE 2024, Portland, USA. https://doi.org/10.1115/IMECE2024-144395

[13] Wang, C., Liu, S., Xia, K., Wang, C., Ye, L. (2024). Numerical research on hydrodynamic performance of toroidal propeller under the influence of geometric parameters. Ocean Engineering, 314: 119704.

https://doi.org/10.1016/j.oceaneng.2024.119704
[14] Jin, J., Ye, Y., Li, X., Li, L., Shan, M., Sun, J. (2023). A mapping model of propeller RANS and LES flow fields based on deep learning methods. Applied Sciences, 13(21): 11716. https://doi.org/10.3390/app132111716
[15] Wilcox, D.C. (2006). Turbulence Modeling for CFD. D C W Industries.
[16] Sikirica, A., Čarija, Z., Kranjčević, L., Lučin, I. (2019). Grid type and turbulence model influence on propeller characteristics prediction. Journal of Marine Science and Engineering, 7(10): 374. https://doi.org/10.3390/jmse7100374
[17] El Hassan, M., Bukharin, N., Alotaibi, N., Matar, M., Assoum, H.H. (2024). CFD study of prism-shaped vortex generators' impact within a coaxial heat exchanger. Mathematical Modelling of Engineering Problems, 11(10): 2657-2663. https://doi.org/10.18280/mmep.111007
[18] Baltazar, J., Melo, D., Rijpkema, D. (2020). Analysis of the blade boundary-layer flow of a marine propeller using a RANS solver. Ocean Engineering, 211: 107633. https://doi.org/10.1016/j.oceaneng.2020.107633
[19] Zhang, W., Ma, N., Gu, X., Feng, P. (2021). RANS simulation of open propeller dynamic loads in regular head waves considering coupled oblique-flow and free-surface effect. Ocean Engineering, 234: 108741. https://doi.org/10.1016/j.oceaneng.2021.108741
[20] Maki, K., Zhao, F., Horn, P., Banks, J., Martio, J., Starke, B., Zaghi, S., Villa, D., Vitola, M., Yoon, H.S., Jiang, Y., Shingo, S. (2024). Practical guidelines for ship CFD applications. International Towing Tank Conference. https://www.ittc.info/media/11958/75-03-02-03.pdf.
[21] Aktas, B., Yilmaz, N., Atlar, M., Sasaki, N., Fitzsimmons, P., Taylor, D. (2020). Suppression of tip vortex cavitation noise of propellers using PressurePoresTM technology. Journal of Marine Science and Engineering, 8(3): 158. https://doi.org/10.3390/jmse8030158
[22] Carlton, J.S. (2019). Propeller performance characteristics. In Marine Propellers and Propulsion, pp. 81-140. https://doi.org/10.1016/B978-0-08-100366-4.00006-7
[23] Viitanen, V., Sipilä, T., Sánchez-Caja, A., Siikonen, T. (2022). CFD predictions of unsteady cavitation for a marine propeller in oblique inflow. Ocean Engineering, 266: 112596. https://doi.org/10.1016/j.oceaneng.2022.112596
[24] Kinaci, O.K., Kukner, A., Bal, S. (2013). On propeller performance of DTC post-Panamax container ship. International Journal of Ocean System Engineering, 3(2): 77-89. https://doi.org/10.5574/IJOSE.2012.3.2.077
[25] Ivagnes, A., Demo, N., Rozza, G. (2024). A shape optimization pipeline for marine propellers by means of reduced order modeling techniques. International Journal for Numerical Methods in Engineering, 125(7): e7426. https://doi.org/10.1002/nme.7426

NOMENCLATURE

J	Advanced coefficient
K_T	Thrust coefficient
K_Q	Torque coefficient
η_0	Open water efficiency
T	Thrust, kg. m. s^{-2}
Q	Torque, kg. m^2. s^{-2}
n	Rotational speed, rpm
D	Propeller diameter, m
V_a	Advanced speed, m. s^{-1}
P/D	Pitch ratio
r/R	Radial position
EAR	Expanded area ratio
S_1, S_2, Tip	Blade segment locations

Greek symbols

ρ	Fluid density, kg. m^{-3}
k	Turbulent kinetic energy, m^2. s^{-2}
ω	Specific dissipation rate, s^{-1}
ϵ	Turbulent dissipation rate, m^2. s^{-3}
β	Turbulent model constant
θ	Angle (skew/rake/pitch), rad
μ	Dynamic viscosity, kg. m^{-1}. m^{-1}
υ	Kinematic viscosity, m^2. s^{-1}